Appl Nanosci
DOI 10.1007/s13204-015-0404-z

ORIGINAL ARTICLE

One-step synthesis of size-controlled CZTS quantum dots

Leena Arora · Vidya Nand Singh · G. Partheepan · T. D. Senguttuvan · Kiran Jain

Received: 6 August 2014 / Accepted: 19 January 2015

Abstract Size-controlled CZTS quantum dots (QDs) were synthesized and its application as a potential electron accepting material for polymer-based hybrid solar cell is demonstrated. The CZTS QDs with a size of 2–10 nm were synthesized in a single step by the decomposition of metal dithiocarbamate and characterized by various techniques; like, SEM, TEM, FTIR, XRD, etc. Results reveal that the CZTS QDs synthesized in oleic acid can quench the luminescence of P3HT effectively. Due to the favourable ionization potential and electron affinity values for CZTS with respect to P3HT, the CZTS QDs act as an effective electron acceptor in the hybrid solar cells based on P3HT/CZTS-QD blends which is also revealed by the charge transfer characteristics of P3HT/CZTS blend.

Keywords CZTS · Low temperature growth · Photovoltaic applications · Quantum dots, P3HT

Introduction

Cu_2ZnSnS_4 (CZTS) is emerging as a promising new sustainable semiconductor material for solar cell applications (Muhunthan et al. 2014; Singh et al. 2015). CZTS has a high absorption coefficient ($\sim 10^4$ cm^{-1}) and an electronic bandgap (~ 1.5 eV) which is nearly ideal for photovoltaics (Katagiri et al. 2008; Muhunthan et al. 2013; Singh et al. 2014). Indeed, thin-film $Cu_2ZnSn(S,Se)_4$ solar cells were recently demonstrated with an overall power conversion efficiency of 12.6 % (Todorov et al. 2010).

To improve upon this result, one potential strategy would be to develop nanostructured CZTS (Dhankhar 2014). For example, semiconductor nanocrystals (or colloidal quantum dots) have been proposed as a general route to high-efficiency, low-cost photovoltaic devices (Klimov 2010; Huynh et al. 2002; Kongkanand et al. 2008). These materials are solution processible and exhibit optical properties that are tunable with nanocrystal size. In materials where the electronic levels can be changed through composition variation and quantum confinement, one can independently control both the effective band gap, and the location of the lowest unoccupied electronic level (e.g. electron affinity). Thus, multilayered devices consisting of films of quantum dots of different sizes could yield inexpensive multijunction solar cells (Franzl et al. 2004). However, the best quantum dot solar cells to date have utilized lead chalcogenide nanocrystals that do not satisfy sustainability goals (Debnath et al. 2010; Luther et al. 2010). CZTS nanocrystals could solve this problem while preserving the advantages of quantum dots.

Most polymer-based solar cells in a bulk architecture have been made by using (6,6)-phenyl-C_{61}-butyric acid methyl ester, (PCBM) as the electron acceptor, resulting in the organic solar cells having a power conversion efficiency (η) up to 5.5 %. When inorganic semiconductor nanocrystals are used as the electron acceptor, the structure is called hybrid solar cells. The hybrid solar cells are promising for future photovoltaic devices, even though the state-of-the-art efficiency of them ($\eta = 2$–3 %) is still rather lower than a polymer/PCBM system. They combine

L. Arora · V. N. Singh (✉) · T. D. Senguttuvan · K. Jain
CSIR-Network of Institutes for Solar Energy, Physics of Energy Harvesting Division, CSIR-National Physical Laboratory, Dr. K. S. Krishnan Marg, New Delhi 110012, India
e-mail: vidyanands@yahoo.com; singhvn@nplindia.org

G. Partheepan
Department of Civil Engineering, MVGR College of Engineering, Vizianagaram 535005, Andhra Pradesh, India

Published online: 13 February 2015

the unique properties of inorganic semiconductors (e.g. high electron mobility, high electron affinity and good stability) with the good film-forming property of conjugated polymers. Moreover, the size, shape, crystallographic structure and the optoelectronic property of semiconductor nanocrystals can be tailored individually during the synthesis process before incorporating the organic polymer. However, one of the major limiting factors leading to low efficiency of polymer-based solar cells is the narrow absorption band of conjugated polymers. Dispersion of inorganic semiconductor QDs with a small band gap organic semiconductor polymer matrices may offer hybrid materials with complementary absorption spectra in the visible spectrum, which has the potential to be used in the development of next-generation photovoltaic devices. However, only a few reports on such hybrid devices are available: CdSe, PbSe or PbS QDs in combination with either poly(2-methoxy-5-(2-ethylhexyloxy)-1,4-phenylene vinylene) (MEH-PPV) or poly(3-hexylthiophene) (P3HT). For the synthesis of CZTS nanoparticles having size smaller than 5 nm, several methods including thermal decomposition of a single-source precursor, photochemical decomposition of single-source precursors, microwave-assisted decomposition of single-source precursors, solvent thermolysis of organometallic precursors, and surfactant-assisted chemical reactions are available.

Herein, we report synthesis of CZTS kesterite phase using metal carbamate as precursors. CZTS having a size of 2–10 nm was obtained depending on the oleic acid content. Upon replacing ligand oleic acid with dodecanethiol, hexagonal phase can be obtained (Arora et al. 2015). CZTS nanoparticles can act as an effective electron acceptor for polymer-based hybrid solar cells with a wide spectral response extending from 300 to 900 nm. The data summarized in this paper show the promise that the molecular precursors such as metal carbamates offers for shape controlled synthesis of potential quantum dot materials at low temperatures for low-cost and high-efficiency solar cell fabrication.

Recently, several synthetic approaches to make CZTS nanocrystals have been reported (Guo et al. 2010; Steinhagen et al. 2009; Riha Riha et al. 2009; Dai Dai et al. 2010). Only a few reports have shown quantum confinement in CZTS nanocrystals, which is critical for exploiting its advantages in solar cells. Secondly, the synthesis methods to grow a controlled size and shape of nanocrystals are limited, which is necessary for not only fundamental studies but also for multijunction photovoltaic architectures. Further, the suitability of these nanomaterials for hybrid solar cell applications has not been well studied. In the present work, we studied the charge transfer characteristics in the blends of P3HT and CZTS by static and dynamic PL measurements to demonstrate the suitability of synthesized nanoparticles for the hybrid solar cell applications. Herein, we are reporting the synthesis of CZTS nanocrystals with varying diameters using a simple route. This allowed us to observe the quantum confinement effect in the optical absorption measurements.

Synthesis of Kesterite-type Cu_2ZnSnS_4 colloidal nanocrystals

CZTS nanocrystals were synthesized using copper, zinc, and tin diethyl dithiocarbamate complexes. Because these molecules decompose thermally to produce corresponding sulfides (Pan et al. 2008); CZTS nanocrystals can be obtained by heating the stoichiometric mixtures of these three complexes. However, since their decomposition temperatures are 220, 240, and 175 °C, respectively, premature decomposition of one can result in unwanted phases such as SnS_2 and Cu_2S. To avoid this; oleylamine was added to lower the decomposition temperature of all of the three complexes and bring them in a narrow temperature range (Jung et al. 2009). The mechanism of oleylamine promoted thermal decomposition of metal alkyldithiocarbamate complexes was proposed by Jung et al. who hypothesized that oleylamine coordinates with the thiocarbonyl carbon of the dithiocarbamate ligand and accelerates decomposition (Jung et al. 2009). Thus, simultaneous decomposition of copper, zinc, and tin dithiocarbamate complexes can be triggered by the sudden injection of oleylamine into a mixture of the three complexes. The amine is added when the mixture temperature is lower than that needed for the decomposition of the individual complexes, but above that needed for the decomposition of the complexes in the presence of the amine.

This approach leads to nucleation and subsequent growth of CZTS nanocrystals. The concentration of the nuclei available for growth is determined by the amount of oleylamine injected. By varying the amount of oleylamine and the growth temperature, we were able to tune the average diameter of the nanocrystals. The final nanocrystal size decreased with an increase in oleylamine concentration and decrease in the growth temperature. The growth time of the nanocrystals did not influence their final size. Attenuated-total-reflection Fourier transform infrared spectra of the nanocrystals showed that the nanocrystals are capped both with oleylamine and oleic acid ligands.

Synthesis of copper diethyldithiocarbamate [Cu $(dedc)_2$]

9.0 g of sodium diethyldithiocarbamate was dissolved in 150 mL of distilled water and added drop-wise to a

solution of 4.23 g of copper chloride in 50 mL distilled water (85 mg/mL) while stirring constantly. The black precipitate formed was filtered and washed multiple times with ultra-high pure water and dried in desiccators. Cu(dedc)$_2$ crystals were dried in vacuum overnight before further use (Khare et al 2011).

Synthesis of zinc diethyldithiocarbamate [Zn (dedc)$_2$]

9.0 g of sodium diethyldithiocarbamate was dissolved in 150 mL of distilled water and added drop-wise to a solution of 3.38 g of zinc chloride in 50 mL of distilled water (68 mg/mL) while stirring constantly. The white precipitate formed was filtered and washed multiple times with ultra-high pure water and dried in desiccators. Zn(dedc)$_2$ crystals were dried in vacuum overnight before further use.

Synthesis of tin diethyldithiocarbamate [Sn (dedc)$_4$]

12.85 g of sodium diethyldithiocarbamate was dissolved in 200 mL of distilled water and added drop-wise to a solution of 2.5 g of tin tetrachloride in 50 mL of distilled water (50 mg/mL) while stirring constantly. The orange precipitate formed was filtered and washed multiple times with ultra-high pure water and dried in desiccators. Orange crystalline powder of Sn(dedc)$_4$ crystals were dried in vacuum overnight before further use.

Synthesis of CZTS nanocrystals

CZTS nanocrystals were synthesized under dry nitrogen atmosphere in a Schlenk line. In a typical synthesis, 18 mL of octadecene and 2 mL of oleic acid were mixed in a 100-mL three-neck flask. 27 mg of Cu (dedc)$_2$, 13.6 nm of Zn(dedc)$_2$, and 26.7 mg of Sn(dedc)$_4$ were then added to this mixture and the flask was connected to the Schlenk line and degassed multiple times at 60 °C. The crystals dissolved on stirring and the solution turned brown. The contents of the flask were heated to the synthesis temperature and a specific volume of oleylamine was injected into the mixture. The nanocrystal size was tuned by changing the temperature and the amount of oleylamine. For example, to carry out synthesis of first sample, 3 mL of oleylamine was injected into the flask at 150 °C to initiate nucleation. The nanocrystals were then allowed to grow for 4 min before quenching the reaction by immersing the flask in water. For the synthesis of second sample, a mixture of 1.5 mL of oleylamine and 1.5 mL of octadecene was injected into the flask at 150 °C. For the synthesis of third and fourth sample, the injection was performed at 175 °C. To avoid premature decomposition of Sn (dedc)$_4$ at this temperature, Sn(dedc)$_4$ was not dissolved and heated in the reaction flask along with other complexes, rather, Sn(dedc)$_4$ was dissolved in oleylamine and octadecene and injected into the flask. All other steps of the synthesis and purification remained the same. Specifically, for third sample, Sn(dedc)$_4$ was dissolved in a mixture of 1.5 mL of oleylamine and 1.5 mL of octadecene and injected into the flask at 175 °C. For fourth sample, Sn (dedc)$_4$ was dissolved in a mixture of 0.75 mL of oleylamine and 2.25 mL of octadecene and injected into the flask at 175 °C. Two more samples were prepared under similar condition as mentioned above but, the synthesis temperature was changed to 175 and 200 °C, respectively, and was stabilized for 30 min.

The nanocrystals were precipitated from the dispersion using reagent grade methanol and were centrifuged for 5 min at 4,000 rpm. The supernatant was discarded and the nanocrystals were redispersed in chloroform. The precipitation and dispersion steps were repeated multiple times to remove excess oleylamine and oleic acid. Finally, the nanocrystals were dispersed in chloroform and stored for later use.

Characterizations

The materials synthesized were characterized using XRD, TEM, SEM, HRTEM, UV absorption, photoluminescence and time-resolved florescence spectroscopy. The X-ray diffraction (XRD) studies were done by using Rigaku Miniflex-II diffractometer (Cu $K\alpha = 1.54$ A°). TEM (transmission electron microscope) studies were carried out using a Tecnai T 30 electron microscope working at 300 kV and scanning electron microscope studies were carried out by using (SEM, Zeiss EV MA-10). For TEM studies, a drop of dispersed solution of the CZTS was carefully transferred to a carbon-coated copper grid followed by evaporation of the solvent. For SEM, a thin gold layer was sputtered on to the film surface. Absorption spectra were recorded using UV 1800 Shimadzu UV spectrophotometer. The photoluminescence measurement was carried out at room temperature using a home-assembled system consisting of a two-stage monochromator, a photomultiplier tube (PMT) with a lock-in amplifier. The PL emission measurements were performed under an excitation wavelength of 405 nm. Fourier transform infrared spectroscopy (FTIR) spectra were recorded with a single beam Perkin Elmer instrument (Spectrum BX-500). This spectrometer allows us to collect spectra in mid-IR, far-IR and near-IR spectral ranges. The spectrum BX contains class II helium neon (HeNe) laser, which emits visible, continuous wave radiation at a wavelength of 633 nm and has a maximum output power of less than 1 mW. The recording abscissa range for measurements was 400–4,000 cm^{-1}. Each spectrum was collected with 64

scans and at 4 cm^{-1} resolution. Time decay measurement was carried out using Edinburgh Laser induspectrom FLS920 (wave length 480 nm pulse width 93.9 nm).

Results and discussion

Thermal decomposition of precursor was studied by thermo-gravimetric analysis (TGA) and differential scanning calorimetry (DSC). Thermo-gravimetric analysis of copper, zinc and tin diethyldithiocarbamate was carried out from room temperature to 300 °C. The TGA curves in Fig. 1a–c show significant weight losses in temperature region 200–300 °C because of thermal decomposition of diethyldithiocarbamate complex. But, as evident from the figures, decomposition is not complete even at 300 °C. The end products are copper, zinc and tin sulfides, respectively, along with volatile compounds. Since the decomposition occurs at around 200 °C, the synthesis was carried out near to this temperature.

The DSC plot in Fig. 1a–c reveals several peak and dips. The sharp dips at temperatures 216 °C in Fig. 1a; 190, 80 and 238 °C in Fig. 1b and 84, 166, 229, 279 °C in Fig. 1c represent that the reaction is endothermic and peaks at temperature 270 °C in Fig. 1c represents that the reaction is exothermic. The enthalpy changes associated with the events are given by the area under the sharp dips.

The formation of CZTS nanoparticles have been confirmed by the Fourier transform infrared (FTIR) spectra as shown in Fig. 2. Band at around 3,073 cm^{-1} indicates the presence of amine group. Peak at 2,919 cm^{-1} is due to –C=CH– stretching mode. Peak at 2,842 cm^{-1} is due to C–H stretching mode. The presence of carbonyl group from carboxyl salt is confirmed by the presence of $–COO^{-}$ symmetric stretch (at approximately 1,446 cm^{-1}) and $–COO^{-}$ asymmetric stretch (at approximately 1,368 cm^{-1}).

The powder X-ray diffraction pattern of the nanocrystalline is shown in Fig. 3. The XRD peaks are broader compared to those for the bulk CZTS which is an indication that the particles are in the nanosize regime. Figure 3a shows the XRD of samples prepared at 150 °C with 1.5 mL oleylamine, b shows the XRD of samples prepared at 175 °C with 1.5 mL oleylamine and c shows the XRD of samples prepared at 175 °C with 0.75 mL oleylamine. All samples are stabilized for 4 min. The XRD pattern exhibits three broad peaks corresponding to the (112), (220) and (312) planes of kesterite CZTS phase, and small intensity peaks corresponding to (101) and (200) also belong to kesterite CZTS [JCPDS card no. 26-0575]. The mean crystallite diameter has been calculated using Scherer formula:

$$d = 0.9\lambda/\beta \mathrm{Cos}\theta \quad (1)$$

where λ is the X-ray wavelength and β is the full width at half maximum. The size of the crystallites was determined using the (112) reflection at 28.91° (2θ) and the calculated values are: 5 nm for (a), 8 nm for (b) and 10 nm for (c).

In order to understand the morphology of as-synthesized CZTS nanoparticles scanning electron microscopic (SEM) study was carried out. Figure 4 shows the typical morphologies of the CZTS films prepared at 175 °C. Large micrometer-sized agglomerates on the film surface were observed. The CZTS nanoparticles are uniformly distributed.

To further investigate the composition of the CZTS, the energy-dispersive X-ray spectroscopic (EDX) spectrum (Fig. 5) was obtained. EDX analysis demonstrates the presence of Cu, Zn, Sn and S. Table in the inset shows relative ratio of Cd: Zn:Sn:S as 2:1:1:4. This ratio agrees with the nominal CZTS stoichiometry.

Transmission electron microscopic (TEM) image and electron diffraction pattern of the CZTS nanoparticles synthesized at 175 °C are shown in Fig. 6. Figure 6a shows the formation of small-sized monodispersed spherical nanoparticles having average size of 4 nm. Figure 6b shows the high magnification image. The presence of sharper lattice fringes in high-resolution image shows good crystallinity of the crystals. The selected area electron diffraction pattern (SAED) of CZTS nanocrystal shown in Fig. 6c shows the presence of (112), (220) and (312) planes of CZTS (corresponding d spacing are 3.18, 1.95 and 1.69 nm, respectively).

In the present study, oleylamine acts as activation agent and oleic acid as the capping agent. Figure 7 shows the absorption spectra of CZTS films synthesized under different conditions as described in experimental part above and the figure caption. A strong blue shift is observed. The band gap energy, E_g, was calculated using the Tauc's relation, $(\alpha h\upsilon)^{1/n} = A\left(h\upsilon - E_g\right)$, where A is a constant and n is equal to 1/2 for direct allowed transitions. The estimation of band gap from the plot of $(\alpha h\upsilon)^2$ vs. $(h\upsilon)$ is shown in Fig. 8. Band gap values are obtained by extrapolating the linear part of the absorption curves to intercept the energy axis $(\alpha h\upsilon = 0)$. In this case, the estimated E_g values are found to vary between 1.36 (bulk) to 2.14 eV for the samples prepared at different conditions (S1–S4) for 4 min. The samples prepared at 175 and 200 °C for 30 min show band gap values of 1.43 and 1.36 eV, respectively. This clearly indicates a considerable decrease in the band gap. Thus, the observed large modification in the band gap confirms strong quantum confinement in this system.

In general, the optical transitions of a bulk semiconductor should shift to higher energy if the optically excited electron hole pair is confined within the nanocrystal boundary (Brus 1984; Lakowicz 1999). The edge of the optical absorption spectrum as well as the lowest energy

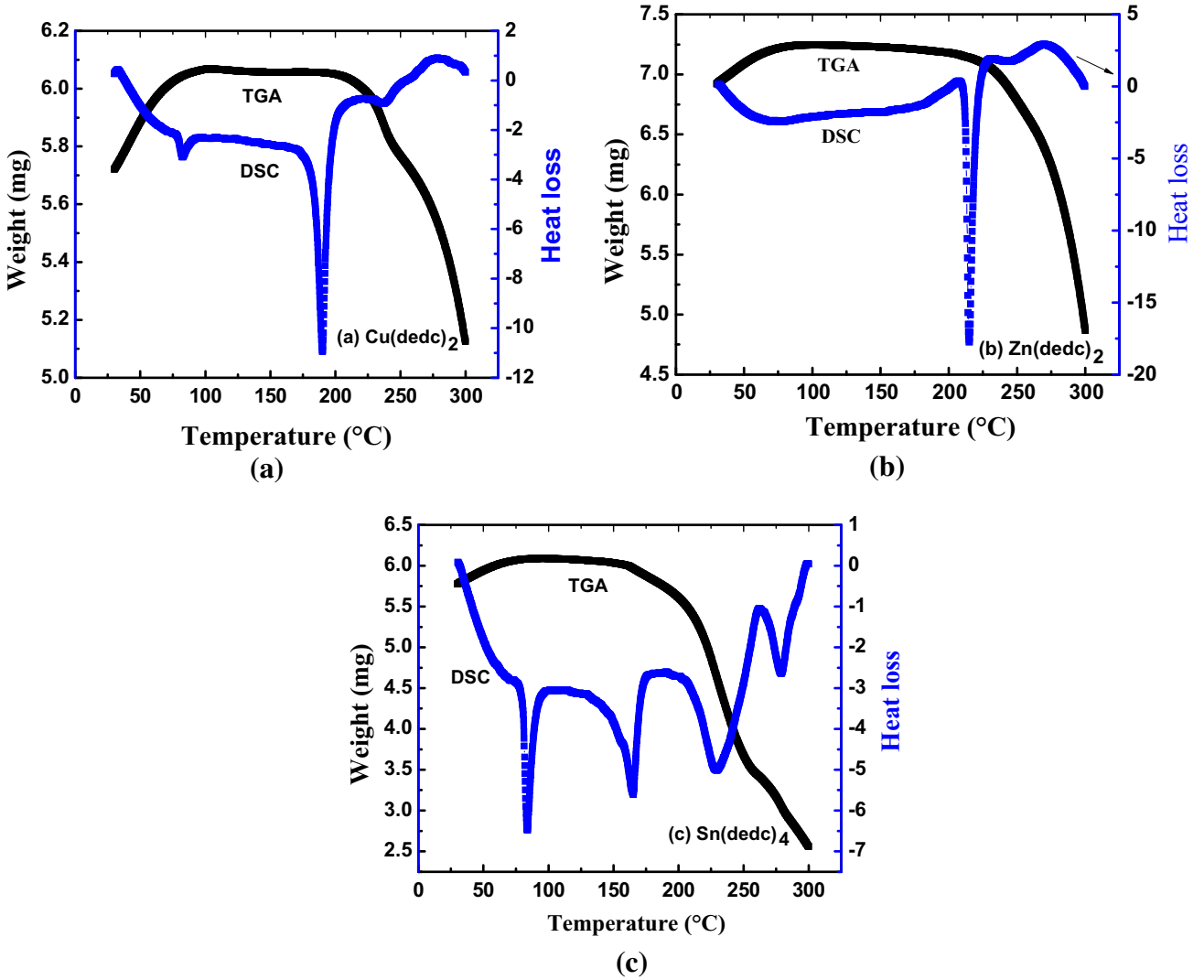

Fig. 1 Thermo-gravimetric analysis and differential scanning calorimetry of **a** copper diethyldithiocarbamate, **b** zinc diethyldithiocarbamate and **c** tin diethyldithiocarbamate

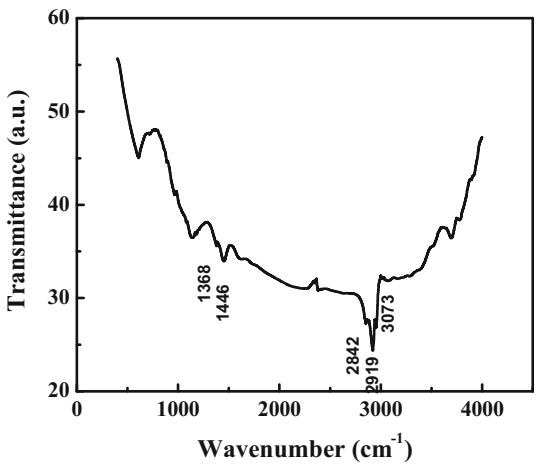

Fig. 2 FTIR Spectrum of CZTS

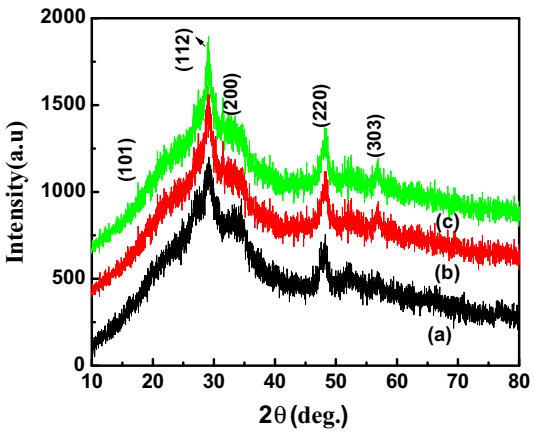

Fig. 3 XRD diffraction patterns of CZTS prepared under different conditions: *a* at 150 °C with 1.5 mL oleylamine, *b* at 175 °C with 1.5 mL oleylamine and *c* at 175 °C with 0.75 mL oleylamine

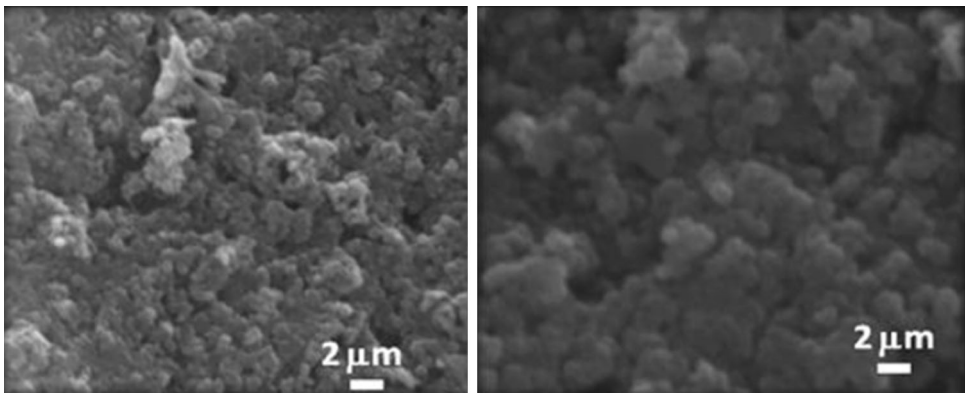

Fig. 4 SEM images of CZTS sample prepared at 175 °C

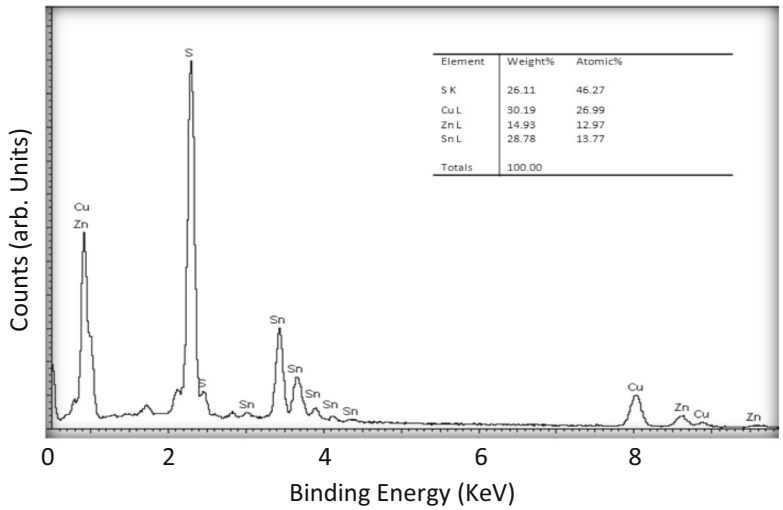

Fig. 5 EDS spectrum of CZTS sample prepared at 175 °C

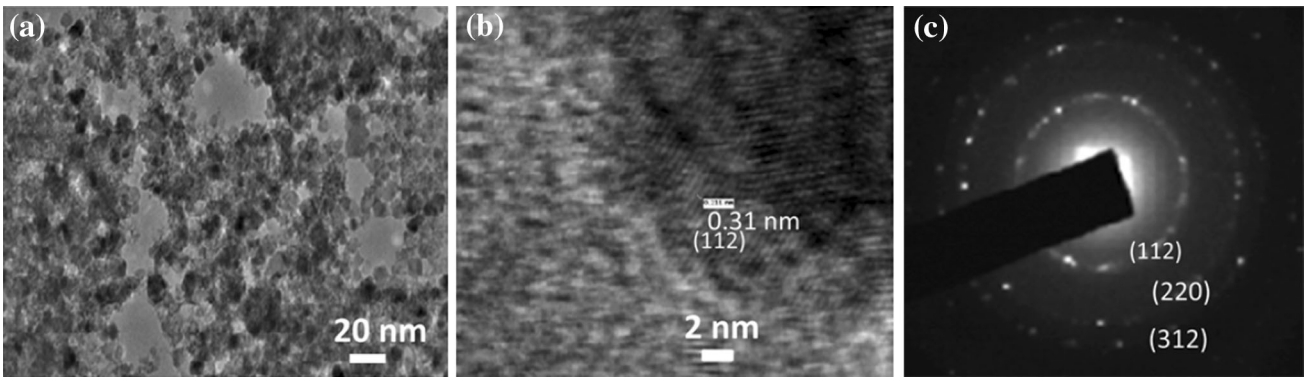

Fig. 6 **a** TEM image, **b** HRTEM image and **c** SAED pattern of CZTS nanoparticles synthesized at 175 °C

absorption peak; shift to higher energy with the decrease in the diameter. No photoluminescence from the CZTS nanocrystals was observed.

Figure 9 shows the PL spectra of the blends of P3HT and CZTS QDs in chloroform, with different P3HT/CZTS-QD ratio. The PL spectra of the blends display an emission profiles similar to the pristine P3HT, which suggests that the remaining luminescence is due to the radiative decay of the excitons from the polymer. A similar conformation of the polymer is indicated for all the solutions, because a change in the conformation of P3HT polymer chains may change the PL spectrum. The PL-quenching efficiency was determined by comparing the maximum emission intensities of the blend samples to that of the pristine P3HT sample. As the concentration of the CZTS QDs increased from 50 to 90 wt%, the yield of the P3HT luminescence decreased substantially from 30 to 70 %. The emission quenching indicates an effective energy transfer from the polymer to the CZTS QDs.

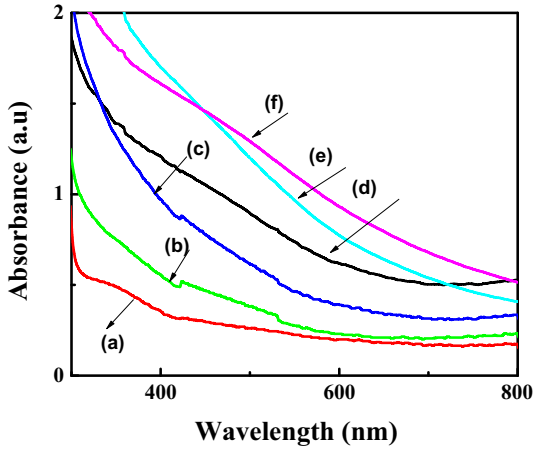

Fig. 7 Absorption spectra of CZTS prepared under different conditions: *a* and *b* are synthesized at 150 °C with different amount of oleylamine and stabilized for 4 min, *c* and *d* synthesized at 175 °C with different amount of oleylamine and stabilized for 4 min, *e* is synthesized at 150 °C and stabilized for 30 min and *f* is synthesized at 175 °C and stabilized for 30 min

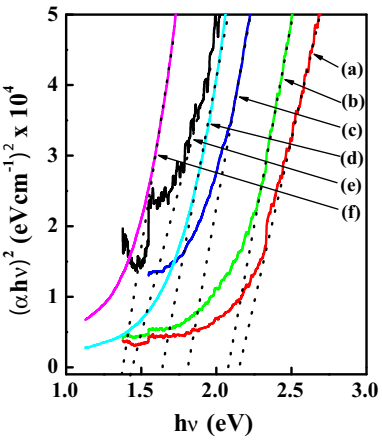

Fig. 8 Estimation of band gap from Tauc's plot

Considering the energy levels of P3HT- and CZTS-QDs, three charge transfer processes are expected. First, as the EA position of P3HT is higher than that of the CZTS QDs, the P3HT/CZTS interface is energetically favourable for the dissociation of photo-generated excitons in P3HT, resulting in the energy transfer from polymer to CZTS QDs, with the electrons being injected into the CZTS QDs (as acceptor) and the holes to remain in the polymer (as donor). This is similar to the well-demonstrated cases of polymer/TiO_2 or polymer/ZnO interfaces. Secondly, CZTS QDs are excited together with the excitation of P3HT, which will lead to the injection of holes onto the polymer and the electrons remaining on the CZTS QDs. Third, since there is a good overlap between the P3HT emission spectrum and the absorption spectrum of CZTS QDs, the exciton transfer from P3HT onto CZTS QDs is possible.

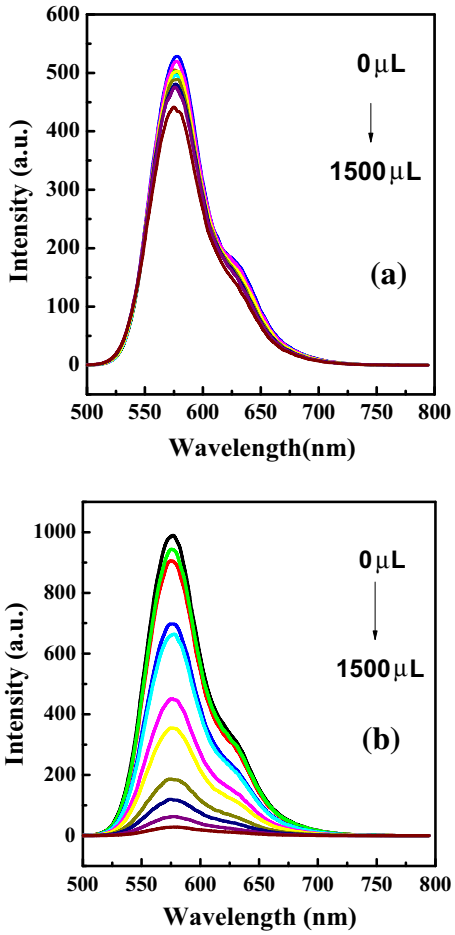

Fig. 9 Emission intensity profiles of P3HT–nanoparticle composite in chloroform in the presence of different concentrations CZTS prepared at two different conditions

Following the exciton transfer, a hole is injected from the CZTS QDs onto the polymer with an electron remaining on the QDs.

Figure 10a, b shows the emission intensity profiles of P3HT:CZTS composite in chloroform as a function of volume of CZTS prepared at two different conditions. As evident in Fig. 10b a more systematic decrease in emission intensity of P3HT:CZTS composite is observed with increase in the CZTS concentration as compared to Fig. 10a. This shows that a more efficient electron transfer, leading to the formation of separated electron–hole pairs that subsequently recombine non-radiatively. It is important to note here that a drastic variation in quenching efficiency of the material was observed with nanoparticle size. For larger size particles (on increasing the size further by increasing the synthesis time to 30 min under experiment 4 conditions), a negligible quenching was observed. Thus large-sized particles do not show much quenching. For a large-sized nanoparticle, the surface where charge transfer is expected to take place is much reduced, as compared to

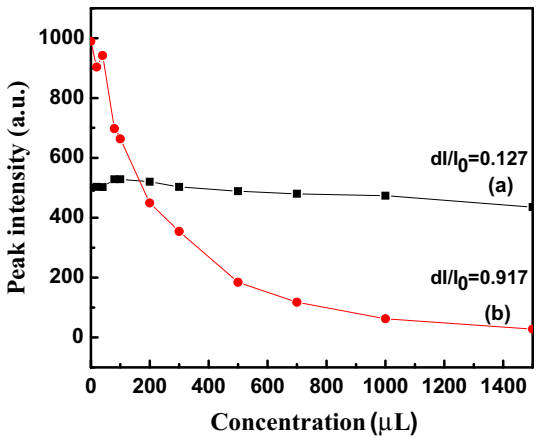

Fig. 10 Emission intensity profile as a function of concentration of CZTS for P3HT:CZTS composite prepared at different conditions

lower sized nanoparticles. If the CZTS nanocrystals were randomly dispersed in the polymer matrix, complete quenching could be expected, as was observed while using 7-nm sized nanoparticles. More than 90 % quenching for 1:10 wt% ratio of polymer to CZTS was observed. The emission intensity profile of P3HT:CZTS composite as a function of concentration of CZTS (Fig. 10) (synthesized at two different conditions) shows the rates of PL decay for P3HT:CZTS is 0.127 for the first synthesis condition and P3HT:CZTS is 0.917 for the second synthesis condition, which confirms the efficient electron transfer in P3HT:CZTS composite.

Luminescence quenching refers to any process that decreases the luminescence intensity of a sample. There are two basic types of quenching: static and dynamic. Both types require an interaction between the fluorophore and quencher. In the case of dynamic quenching, the quencher must diffuse to the fluorophore during the lifetime of the excited state. Upon contact, the fluorophore returns to the ground state without emission of a photon. In the case of static quenching, a complex forms between the fluorophore and the quencher, and this complex is nonfluorescent. The formation of this complex does not rely upon the population of the excited state.

In the simplest case of collisional quenching, the Stern–Volmer equation can be written as:

$$I_0/I = 1 + K_{sv}[Q], \tag{2}$$

where I_0 and I are the fluorescence intensities observed in the absence and presence of quencher, respectively, $[Q]$ is the quencher concentration, and K_{SV} is the Stern–Volmer quenching constant. In the simplest case, a plot of I_0/I vs. $[Q]$ should yield a straight line with a slope equal to K_{SV}. Such a plot known as a Stern–Volmer plot is shown in Fig. 11a, b for P3HT:CZTS nanocomposites synthesized at two different conditions. However, as evident from

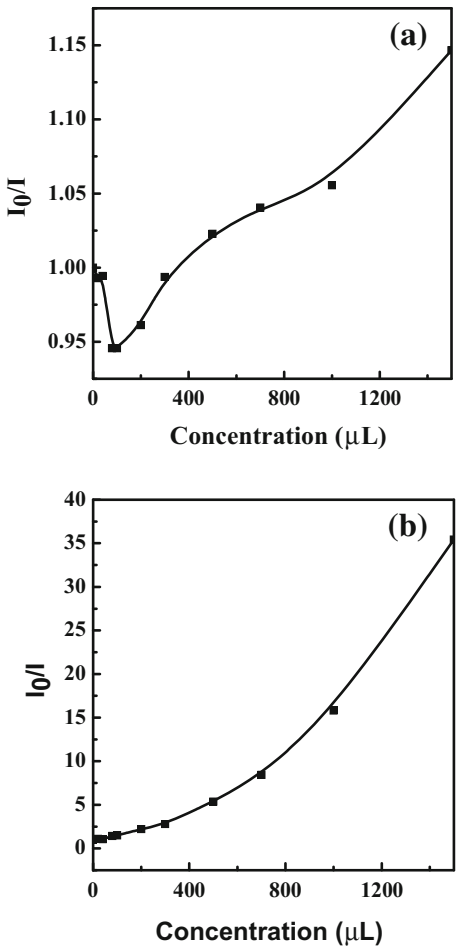

Fig. 11 Stern–Volmer plots of P3HT:CZTS nanocomposite prepared at different conditions

Fig. 11a, b, nonlinear Stern–Volmer plots with negative deviation from linearity are observed. Such nonlinear Stern–Volmer plots can occur in the case of heterogeneous quenching (collisional or static) if some of the fluorophores are less accessible than others (Brus 1984; Lakowicz 1999). The Stern–Volmer quenching constant for P3HT:CZTS is 0.1504×10^3 M^{-1} for first synthesis condition and 10.9×10^3 M^{-1} for second synthesis condition, respectively. Here, it is evident that P3HT:CZTS nanocomposites, show higher values of quenching constants (i.e. high rate of quenching) for second synthesis condition resulting in efficient charge transfer across P3HT:CZTS nanocomposites.

In order to understand the electron transfer dynamics, lifetime measurement studies were performed. Figure 12 shows the PL decay curve for P3HT and for P3HT–CZTS nanocomposites.

The PL decay times at which the PL intensity decreases to $1/e$ of its initial value are used to compare the life time of P3HT and P3HT–CZTS.

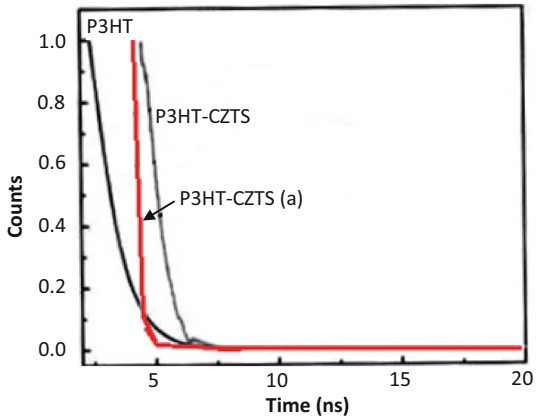

Fig. 12 TRF spectra for P3HT and P3HT–CZTS (at different conditions)

Table 1 Lifetime of P3HT and P3Ht–CZTS composite samples

	Γ (ns)
P3HT	0.92115
P3HT–CZTS	0.748
P3HT–CZTS	0.13485

The emission intensity recorded at the emission maximum exhibited monoexponential decay

$$I(t) = A\exp(-t/\Gamma), \quad (3)$$

where I is the normalized emission intensity, A is the pre-exponential factor, t is the time after pulsed-laser excitation, and Γ is lifetime. The decay of both samples is fitted with single exponential. Excitation wavelength used during measurements is 480 nm. The kinetic parameters of the P3HT and P3HT–CZTS emission decay analysis are summarized in Table 1. These results show that the life time of P3HT decreases from 0.9 to 0.135 ns on addition of CZTS indicating efficient charge transfer in P3HT–CZTS nanocomposites (with CZTS synthesized at two different temperatures, 150 and 175 °C).

Conclusion

CZTS QDs with a size of 2–7 nm have been successfully synthesized using OA. Due to the favourable IP and EA positions with respect to the P3HT, the CZTS QDs act as an effective electron acceptor for the hybrid solar cells based on the P3HT/CZTS-QD blends, by allowing the efficient charge separation for neutral excited states produced either on the polymers or on the QDs. The promise of the present synthesis approach to prepare CZTS QDs may provide a potential QD material for low-cost and high-efficiency solar cell fabrication. Further, the average nanocrystal diameter could also be tuned. Characterization using HRTEM, XRD, and SEM confirm the phase purity of the CZTS nanocrystals. Our smallest nanocrystals exhibit shifts in their optical transitions due to quantum confinement. In summary, nanocrystalline CZTS has been colloidally synthesized through a facile greener and inexpensive route, which involves the surfactant-assisted thermolysis of metal dithiocarbamates.

References

Arora L, Gupta P, Chhikara N, Singh OP, Muhunthan N, Singh VN, Singh BP, Jain K, Chand S (2015) Green synthesis of wurtzite copper zinc tin sulfide nanocones for improved solar photovoltaic utilization. Appl Nanosci 5(2):163–167

Brus LE (1984) Electron–electron and electron-hole interactions in small semiconductor crystallites: the size dependence of the lowest excited electronic state. J Chem Phys 80(9):4403–4409

Dai P, Shen X, Lin Z, Feng Z, Xu H, Zhan J (2010) Band-gap tunable $(Cu_2Sn)_{x/3}Zn_{1-x}S$ nanoparticles for solar cells. Chem Commun 46(31):5749–5751

Debnath R, Tang J, Barkhouse DA, Wang X, Pattantyus-Abraham AG, Brzozowski L (2010) Ambient-processed colloidal quantum dot solar cells via individual pre-encapsulation of nanoparticles. J Am Chem Soc 132(17):5952–5953

Dhankhar M, Singh OP, Singh VN (2014) Physical principles of losses in thin film solar cells and efficiency enhancement methods. Ren Sustain Energy Rev 40:214–223

Franzl T, Klar TA, Schietinger S, Rogach AL, Feldmann J (2004) Exciton recycling in graded gap nanocrystal structures. Nano Lett 4(9):1599–1603

Guo Q, Ford GM, Yang WC, Walker BC, Stach EA, Hillhouse HW, Agrawal R (2010) Fabrication of 7.2 % efficient CZTSSe solar cells using CZTS nanocrystals. J Am Chem Soc 132(49):17384–17386

Huynh WU, Dittmer JJ, Alivisatos AP (2002) Hybrid nanorod-polymer solar cells. Science 295(5564):2425–2427

Jung YK, Kim JI, Lee JK (2009) Thermal decomposition mechanism of single-molecule precursors forming metal sulfide nanoparticles. J Am Chem Soc 132(1):178–184

Katagiri H, Jimbo K, Yamada S, Kamimura T, Maw WS, Fukano T et al (2008) Enhanced conversion efficiencies of Cu_2ZnSnS_4-based thin film solar cells by using preferential etching technique. Appl Phys Express 1(4):041201

Khare A, Wills AW, Ammerman LM, Norris DJ, Aydil ES (2011) Size control and quantum confinement in Cu_2ZnSnS_4 nanocrystals. Chem Commun 47(42):11721–11723

Klimov VI (2010) Nanocrystal Quantum Dots. CRC Press, Boca Raton

Kongkanand A, Tvrdy K, Takechi K, Kuno M, Kamat PV (2008) Quantum dot solar cells. Tuning photoresponse through size and shape control of CdSe-TiO_2 Architecture J Am Chem Soc 130(12): 4007–4015

Lakowicz JR (1999) Principles of Fluorescence spectroscopy. Kluwer Academic/Plenum, New York

Luther JM, Gao J, Lloyd MT, Semonin OE, Beard MC, Nozik AJ (2010) Stability assessment on a 3 % bilayer PbS/ZnO quantum dot heterojunction solar cell. Adv Mater 22(33):3704–3707

Muhunthan N, Singh OP, Singh S, Singh VN (2013) Growth of CZTS thin films by co-sputtering of metal targets and sulfurization in H_2S. Inter J Photoenergy 2013:752012

Muhunthan N, Singh OP, Thakur MK, Karthikeyan P, Singh D, Saravanan M, Singh VN (2014) Interfacial properties of CZTS thin film solar cell. J Sol Energy 2014:476123

Pan D, An L, Sun Z, Hou W, Yang Y, Yang Z, Lu Y (2008) Synthesis of Cu-In-S ternary nanocrystals with tunable structure and composition. J Am Chem Soc 130(17):5620–5621

Riha SC, Parkinson BA, Prieto AL (2009) Solution-based synthesis and characterization of Cu_2ZnSnS_4 nanocrystals. J Am Chem Soc 131(34):12054–12055

Singh OP, Muhunthan N, Singh VN, Samanta K, Dilawar N (2014) Effect of temperature on thermal expansion and anharmonicity in Cu_2ZnSnS_4 thin films grown by co-sputtering and sulfurization. Mater Chem Phys 146(3):452–455

Singh OP, Muhunthan N, Singh VN, Singh BP (2015) Effect of annealing time on the composition, microstructure and band gap of copper zinc tin sulfide thin films. Adv Mater Lett 6(1):2–7

Steinhagen C, Panthani MG, Akhavan V, Goodfellow B, Koo B, Korgel BA (2009) Synthesis of Cu_2ZnSnS_4 nanocrystals for use in low-cost photovoltaics. J Am Chem Soc 131(35): 12554–12555

Todorov TK, Reuter KB, Mitzi DB (2010) High-efficiency solar cell with earth-abundant liquid-processed absorber. Adv Mater 22:E156–E159